Instability Analysis of Supercritical CO? during Transportation and Injection in Carbon Capture and Storage Systems

Authors:

Il Hong Min, Seong-Gil Kang, Cheol Huh

Date Submitted: 2018-09-21

Keywords: carbon capture and storage (CCS), CO2 pipeline, stability map, flow instability, supercritical CO2

Abstract:

Captured CO? is in a subcritical state, whereas CO? deep underground is in a supercritical state because of the high geothermal heat and pressure. The properties of CO? can change rapidly at the critical point and in the near-critical region during the transportation and injection process. This study aims to identify the instabilities in the CO? flow in these regions, along with the causes and effects, during the transportation and injection process, and propose relevant design specifications. Thus, the critical points and near-critical region of CO? flow were numerically analyzed. The unstable region is presented in terms of temperature and pressure ranges, and the changes in the CO? properties in this region were analyzed. In the unstable region, the sudden change in density was similar to the density wave oscillation of a two-phase flow. The CO? stability map we obtained and the stability map of supercritical water show similar trends. Flow instability was also found to occur in standard CO? transportation pipelines. We demonstrate that flow instability in CO? transportation and injection systems can be avoided by maintaining the proposed conditions.

Record Type: Published Article

Submitted To: LAPSE (Living Archive for Process Systems Engineering)

Citation (overall record, always the latest version):	LAPSE:2018.0562
Citation (this specific file, latest version):	LAPSE:2018.0562-1
Citation (this specific file, this version):	LAPSE:2018.0562-1v1

DOI of Published Version: https://doi.org/10.3390/en11082040

energies

MDPI

Article

Instability Analysis of Supercritical CO_2 during Transportation and Injection in Carbon Capture and Storage Systems

Il Hong Min [1], Seong-Gil Kang [2] and Cheol Huh [1,*]

[1] Department of Convergence Study on the Ocean Science and Technology, Ocean Science and Technology School, Korea Maritime and Ocean University, Busan 49112, Korea; ihmin@kmou.ac.kr
[2] Korea Research Institute of Ships and Ocean Engineering, Daejeon 34103, Korea; kangsg@kriso.re.kr
* Correspondence: cheolhuh@kmou.ac.kr; Tel.: +82-51-410-5247

Received: 16 July 2018; Accepted: 3 August 2018; Published: 6 August 2018

Abstract: Captured CO_2 is in a subcritical state, whereas CO_2 deep underground is in a supercritical state because of the high geothermal heat and pressure. The properties of CO_2 can change rapidly at the critical point and in the near-critical region during the transportation and injection process. This study aims to identify the instabilities in the CO_2 flow in these regions, along with the causes and effects, during the transportation and injection process, and propose relevant design specifications. Thus, the critical points and near-critical region of CO_2 flow were numerically analyzed. The unstable region is presented in terms of temperature and pressure ranges, and the changes in the CO_2 properties in this region were analyzed. In the unstable region, the sudden change in density was similar to the density wave oscillation of a two-phase flow. The CO_2 stability map we obtained and the stability map of supercritical water show similar trends. Flow instability was also found to occur in standard CO_2 transportation pipelines. We demonstrate that flow instability in CO_2 transportation and injection systems can be avoided by maintaining the proposed conditions.

Keywords: supercritical CO_2; flow instability; stability map; CO_2 pipeline; carbon capture and storage (CCS)

1. Introduction

Carbon capture and storage (CCS) is a technology used to capture CO_2 emissions from power plants or industrial facilities to reduce greenhouse gas emissions; the gas is subsequently injected and stored in depleted oil and gas reservoirs or saline aquifers [1].

The total value chain of CCS technology comprises capture, transportation, injection, and storage. The CO_2 captured in power plants or industrial facilities is in a subcritical state. However, the CO_2 stored deep underground is maintained in a supercritical state because of the high geothermal heat and pressure in the reservoir. This implies that the operating conditions associated with the critical point and near-critical regions may occur during the transportation and injection processes, which are intermediate steps, because of the phase difference between the captured CO_2 and stored CO_2. In a previous study [2–4] by the authors of this paper, a depleted gas field in the East Sea of Korea was studied as a storage reservoir. Near-critical point flow and supercritical state flow of CO_2 were found to occur in the topside pipeline of the offshore platform and the upper part of the injection wellbore at a specific injection point, thereby causing flow instability in the pipeline [5]. Such flow instability can cause an additional pressure drop in the pipeline or disable flow control. Therefore, the near-critical point and supercritical state flows of CO_2 should be considered in the initial design stage to allow the safe and economic injection and storage of CO_2 in CCS systems. To this end, the properties and flow

characteristics of CO_2 at the critical point and in the near-critical region must be studied thoroughly. The purpose of this study is to identify the instability in the CO_2 flow at the critical point and in the near-critical region during the transportation and injection processes for CCS, to analyze the cause and effect of the flow instability, and to propose design specifications that reflect the results of the analysis.

Previous studies on the properties and flow instability of supercritical fluids similar to the case employed in this study can be categorized into four areas. The first area of study pertains to the critical and pseudocritical states of single-component fluids. Pioro and Mokry [6] presented the terms and definitions for critical and supercritical fluids. The saturation line of fluids such as pure water or CO_2 is a single line, and the pressure and temperature of CO_2 at the critical point are 73.8 bar and 30.9 °C, respectively. In a particular part of the supercritical region above the critical point, the properties of the single-component fluid change abruptly at a particular pressure and temperature, and this is defined as the pseudocritical point. Furthermore, more than one pseudocritical point can exist, and the line connecting these points is called the pseudocritical line [7]. Every pseudocritical temperature in the pseudocritical line has a corresponding pseudocritical pressure. Figure 1 shows the phase envelope of CO_2 which was calculated using NIST's REFPROP [8]. As shown in Figure 1, the pseudocritical line tends to extend from the saturation line of CO_2 in the subcritical state to the supercritical state via the critical point. The specific heat, density, and enthalpy of the supercritical CO_2 change drastically near the pseudocritical line [9]. The abrupt behavior of the properties at the pseudocritical line tends to decrease further from the critical point [10]. In the case of the phase envelope of natural gas, as shown in Figure 2 (which was calculated using NIST's REFPROP [8]), the saturation line takes the form of a parabola because the gas comprises a hydrocarbon mixture, unlike CO_2.

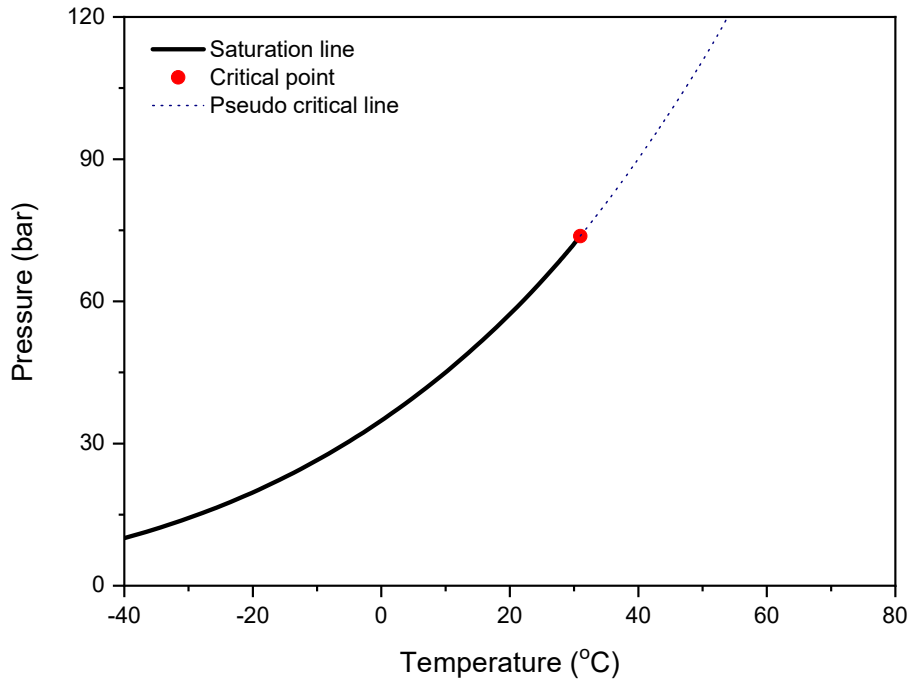

Figure 1. Phase envelope of pure CO_2.

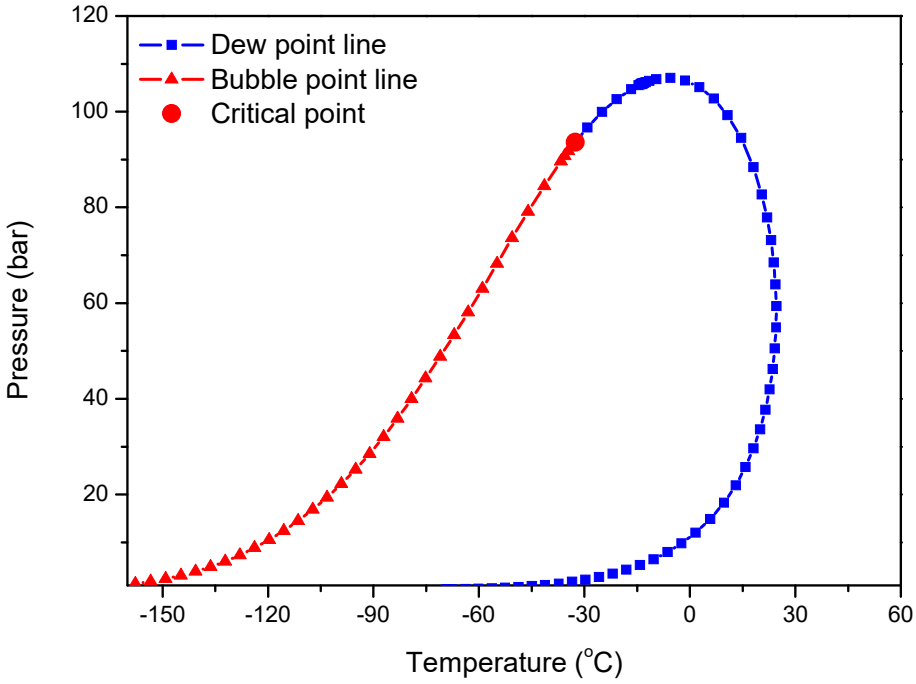

Figure 2. Phase envelope of natural gas.

Although the phase behavior of natural gas has been thoroughly studied, studies of the phase behavior of CO_2 are lacking. Shoaib et al. [11] investigated the effects of the operating conditions on the dew point and condensation rate of natural gas and developed two quadratic equations to relate them to the operational variables of the dew point control unit (DPCU). Guerrero-Zárate et al. [12] developed and validated a new algorithm to determine the critical point of a natural gas mixture. Wang et al. [13] derived implicit curve-fitting equations to increase the speed of calculation of natural gas properties in the supercritical pressure region. In summary, there is an abundance of knowledge and experience regarding the transportation of natural gas through pipelines [14–17]. However, it is difficult to analyze the phase transition in the transport of CO_2, which is the objective of this study, because of the single saturation line. Moreover, the behavior of near-critical point flow is significantly more complicated than that of a natural gas flow.

The second area of study relates to the flow of supercritical CO_2 and the application of supercritical and pseudocritical CO_2 to thermodynamic cycles. Ma et al. [18] conducted a study to improve the performance of the Brayton cycle using the thermodynamic properties of pseudocritical CO_2. Shao and Zhang [19] considered the saturation temperature of subcritical state CO_2 as the pseudocritical temperature of supercritical state CO_2 and proposed the possibility of using supercritical state CO_2 in the CO_2 cycle by extending the vapor pressure equation. Gupta et al. [20] established a correlation between the heat transfer characteristics based on the experimental pseudocritical CO_2 data obtained for a supercritical region flow in a vertical tube. They applied the correlation to the Brayton gas turbine cycle. In addition, active studies have been carried out to apply the rapidly increasing specific heat and heat transfer coefficient of pseudocritical CO_2 in the supercritical region to the working fluid of the cycle [21–24]. However, most studies have focused solely on the analysis of thermodynamic properties, with relatively few studies considering the flow instability of supercritical state CO_2. Furthermore, because the experimental cycle used for analysis is small compared to a CCS transportation system, wherein the pipelines are on the order of several tens to several hundreds of kilometers, the results are limited in their extension to the CO_2 transportation pipelines employed in CCS technologies.

The third area of study is the flow instability of fluids at supercritical and near-critical points in the natural circulation loops used to cool nuclear power systems. Archana et al. [25] experimented with and analyzed the transient flow of supercritical CO_2 in a natural circulation loop. Chen et al. [26]

performed a numerical analysis on the flow instability arising from rapid changes in the properties of pseudocritical state CO_2 in a natural circulation loop. Other experiments and numerical analyses have been conducted to analyze the flow instability of supercritical CO_2 in a natural circulation loop [27–29]. These studies have investigated the instability of supercritical CO_2 flow, similar to that in this study. However, for the natural circulation loop considered in their studies, the driving force of the flow is the buoyancy arising from the density difference, whereas the driving force of the flow in a long-distance CO_2 pipeline is the pressure difference. Therefore, it is difficult to use the results of their studies for the CO_2 transportation and injection processes in CCS. Moreover, the scale of the system is different.

The fourth area of study regarding the flow instability of supercritical fluids is the flow instability of supercritical water caused by the density wave oscillations that occur near the pseudocritical line. The density and compressibility factor of supercritical water change suddenly along the pseudocritical line, resulting in unstable fluid behavior [30]. Ambrosini [31] argued that the flow instability of supercritical water in heated channels is similar to the flow instability caused by the two-phase flow of subcritical water. The similarity in the obtained stability maps validated the results. Xiong et al. [32] investigated the flow instability of supercritical water flowing in a vertical pipeline and analyzed the main parameters causing flow instability. However, the critical pressure and temperature of water differ from those of CO_2, and the changes in the properties are different in terms of the critical temperature and pressure. Therefore, it is difficult to apply these values to the CO_2 transportation and injection processes of a CCS system.

As mentioned above, to implement CCS technology efficiently, the near-critical state flow and the supercritical state flow of CO_2 must be considered. However, existing studies have not thoroughly analyzed the flow instability caused by near-critical or supercritical CO_2 flows. Therefore, in this study, a numerical analysis was conducted, focusing on the flow instability caused by the operating conditions associated with near-critical point and supercritical states in a CO_2 transportation and injection system.

2. Method of Numerical Analysis

2.1. CCS Chain Configuration

A CO_2 transportation and injection system model was made using four components: a subsea pipeline, a riser, a topside pipeline, and a wellbore. It was assumed that the CO_2 captured in onshore power plants is temporarily stored in a hub terminal near the storage site [3,33]. The CO_2 at the hub terminal is then transported through the subsea pipeline to the sea of the reservoir, and the transported CO_2 is elevated to the offshore platform using the riser. The injection equipment on the topside of the offshore platform comprises a heater, a choke valve, metering devices, monitoring devices, and isolation devices. The CO_2 is transferred from the injection facility on the offshore platform to the sub-seabed through the injection riser and is injected from the sub-seabed to the reservoir using the injection wellbore. Figure 3 shows the overall configuration of the transportation and injection system [3,33].

In this study, the possibility, causes, and effects of flow instability when CO_2 in the topside pipeline and injection wellbore flows in near-critical and supercritical states were analyzed using numerical analysis. OLGA 2014.1 [34] was used for this purpose. The CO_2 in a CCS system is assumed to have a purity of 99% or more. The properties of pure CO_2 were used to determine the behavior of supercritical state CO_2 near the critical point from a single saturation line accurately. The single component module (OLGA) was used to simulate the behavior of pure CO_2 in the system [35].

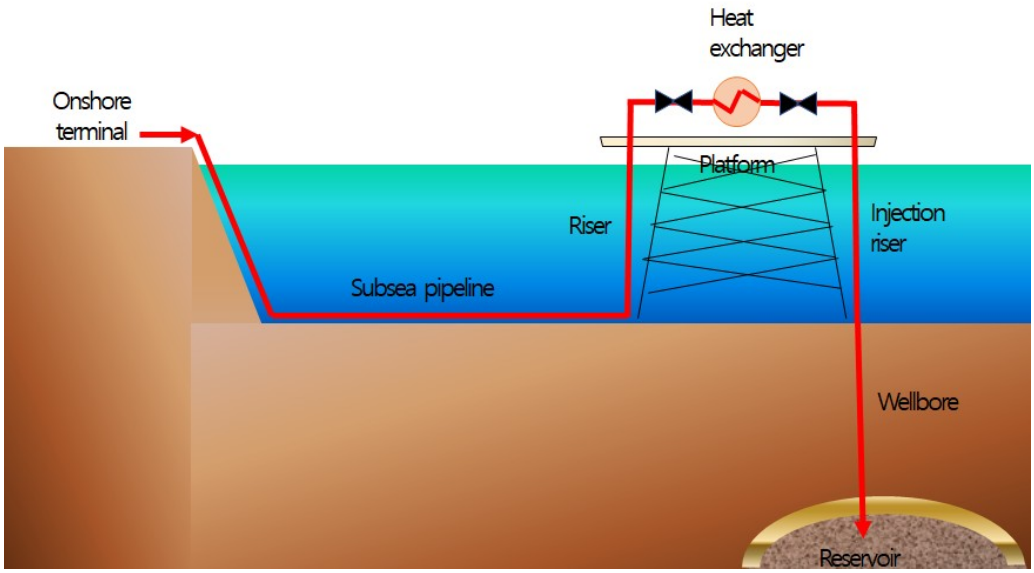

Figure 3. Schematic of the offshore CO_2 transportation and injection system.

The numerical methods and mathematical descriptions were described in the previous study [35] of the authors. The pipeline was designed to be installed in the sub-seabed approximately 60 km from the coastal terminal to the sea where the platform is installed. The riser was designed to have a length of 155 m, measuring from the end of the seabed pipeline to the topside of the offshore platform and considering the seawater depth of the reservoir area. The topside pipeline was approximately 1 km in length and was equipped with isolation valves, a heat exchanger for heating, and choke valves. The injection wellbore comprises a seawater injection riser, which connects the platform to the sub-seabed, and an underground injection wellbore. The length of the underground injection wellbore was designed such that it could be installed vertically to a depth of approximately 2438 m, measuring from the sub-seabed to the storage reservoir.

2.2. Calculation Conditions

Table 1 lists the main calculation conditions for the transportation and injection system proposed in this study. The inside diameter of the pipeline was 8 in (20.32 cm). The same value was used for the entire system including for the subsea pipeline, riser, topside pipeline, and injection wellbore. The inner diameter was selected considering the flow rate, pressure drop, heat transfer, and erosional velocity ratio (EVR), as given in the previous study of the authors [33].

Table 1. Calculation conditions for the numerical simulation.

Calculation Condition	Design Value
CO_2 composition	Pure CO_2
CO_2 flow rate	31.5 kg/s
Pipeline diameter	8 in
Topside arrival temperature of CO_2	5.7 °C
Reservoir temperature	97.8 °C
Length of the topside pipeline	1000 m
Length of wellbore	2438 m

For the numerical analysis of the CO_2 flow in the transportation and injection system, the effect of the increase in the reservoir pressure caused by CO_2 injection on the system should be considered. The pressure of the reservoir increases over the injection period because of the accumulation of CO_2 in

the reservoir. The correlation between the pressure change in the reservoir and the bottom hole and the injection rate of CO_2 over time was obtained through reservoir simulation [36].

As shown in Figure 4, the bottom hole pressure increased over an injection period of 120 months because of the accumulation of injected CO_2. The pressure of the entire transportation and injection system increased because of the increased bottom hole pressure, eventually making the flow in a specific section of the system enter the supercritical state.

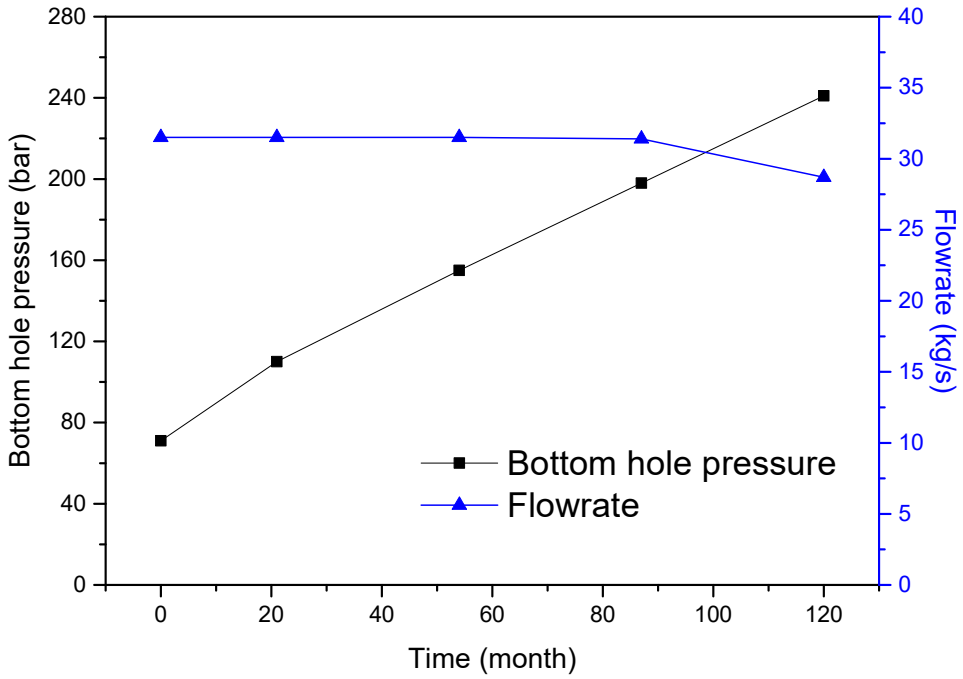

Figure 4. Variations in the reservoir pressure, bottom hole pressure, and flow rate over the injection period.

In the previous study by the authors, the operating pressure near the CO_2 critical pressure (Pc = 73.8 bar) occurred at the topside during the injection period (approximately 54 months), and the temperature of the CO_2 arriving at the topside was calculated to be 5.7 °C [5]. When the topside CO_2 was heated to a near-critical temperature (Tc = 30.9 °C) using the heater, the flows in the topside pipeline and injection wellbore became unstable.

To analyze the CO_2 flow instability, simulations were performed by varying the temperature and pressure. The bottom hole pressure was controlled to allow the operating conditions to reach the critical pressure in the topside pipeline. The heating temperature of the topside heater at each bottom hole pressure was set near the critical temperature (30 to 40 °C). In particular, numerical analysis was carried out for 20 cases, wherein the heating temperature of the heater was increased by 1 °C from 30 to 40 °C in each of the 10 cases and was decreased by 1 °C from 40 to 30 °C in an additional 10 cases. The generation of the transient state was checked while maintaining the temperature condition for 100 h, i.e., by calculation for a sufficient time. Furthermore, to eliminate the influence of the rapid temperature change, the time required to increase or decrease the temperature by 1 °C was set to 10 h.

Figure 5 shows the heating temperature of the heater with respect to the simulation time. Because detailed information concerning the internal configuration of the heater is unavailable at this stage, it was assumed that the pressure drop generated through the heater was negligible. In addition, the pressure, temperature, and density of the CO_2 at the heater outlet were analyzed to verify the flow instability after heating using the topside heater. Table 2 lists the bottom hole pressure, topside operating pressure, and heater set temperature for each numerical analysis case.

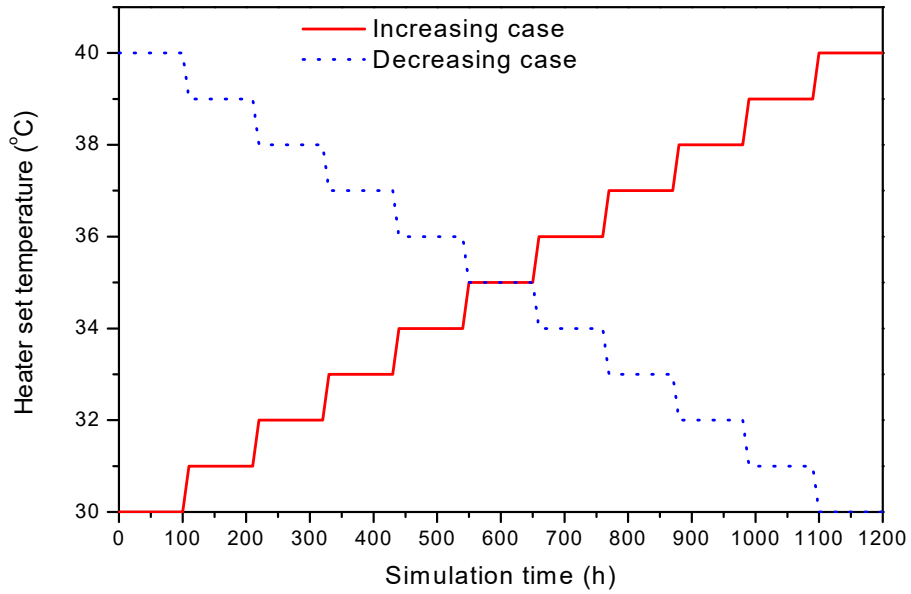

Figure 5. Variation in the heater set temperature with respect to the simulation time.

Table 2. Operating conditions for each calculation case.

Case	Bottom Hole Pressure (bar)	Topside Operating Pressure (bar)	Increase Heater Set Temperature (°C)	Decrease Heater Set Temperature (°C)
1	170	70–76	30–40	40–30
2	180	72–78		
3	190	73–79		
4	200	74–80		
5	210	77–83		
6	220	78–84		
7	230	80–86		
8	240	82–88		
9	250	84–90		
10	260	85–91		

3. Results

3.1. Identification of the Unstable Region

Figure 6 shows the calculation results for case 4 as an example. The density, pressure, and temperature of CO_2 were analyzed at the outlet of the heater. The outlet conditions of the heater include a pressure of 79 bar and a temperature of 37 °C, which are higher than those at the critical point of CO_2 (Pc = 73.8 bar and Tc = 30.9 °C). Under these operating conditions, the heater set temperature gradually decreases and approaches the critical point operating condition. When the simulation time is longer than 250 h, the operating pressure and temperature of the heater outlet are approximately 75 bar and 35 °C, respectively. At this point, the density and pressure of the CO_2 at the heater outlet start to vary. In this study, the operating conditions associated with the flow instability at the near-critical point were confirmed for all cases listed in Table 2. In every case, the flows destabilized because of the fluctuations in the density, pressure, and temperature when the operating conditions were closer to the critical point. In this study, the conditions for the occurrence of flow instability were determined when the density variation was ±50 kg/m^3 or more at a steady state. Furthermore, the pressure and temperature at this time were considered operating conditions, causing flow instability in the pipeline. The temperature and pressure at which the flow started to destabilize were obtained for each case listed in Table 2. The region of flow instability was determined for the critical point, near-critical region, near the pseudocritical line region, and supercritical region.

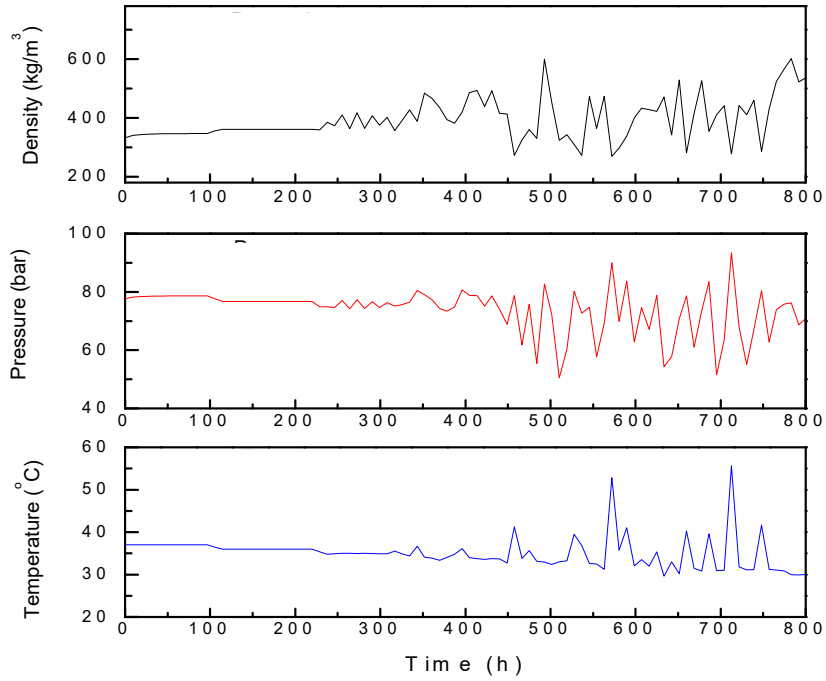

Figure 6. Simulation results of case 4 (reduction in heater temperature).

The pressure and temperature at which the flow begins to destabilize can be found using the pressure–temperature diagram of CO_2 by combining the aforementioned simulation results. Figure 7 shows the results, wherein the pressure and temperature ranges are indicated. The unstable region is highlighted as the colored region in Figure 7. Furthermore, the instability boundaries which were obtained through the numerical simulations are also specified.

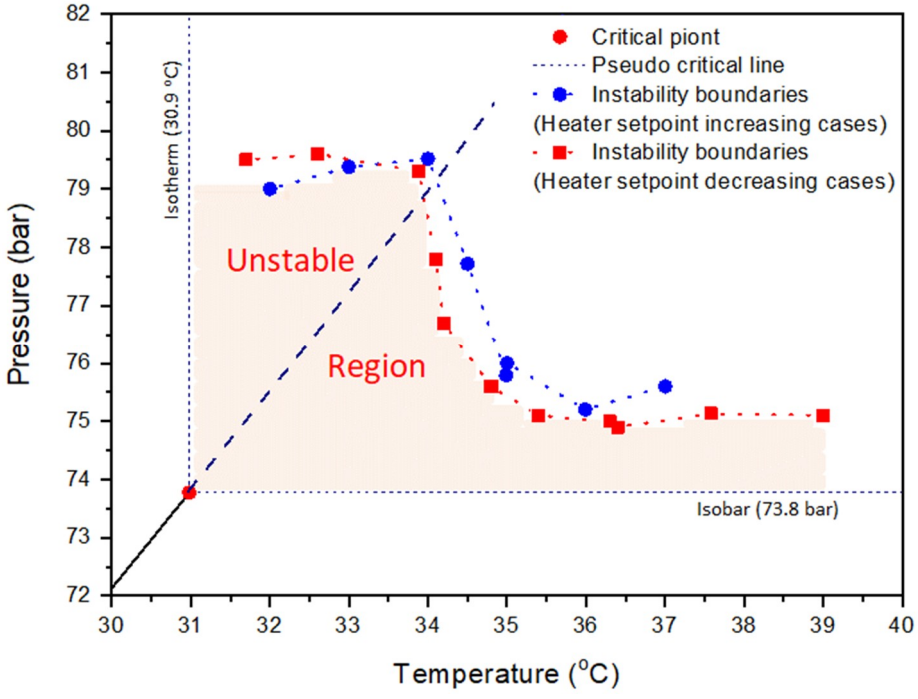

Figure 7. Unstable region of supercritical CO_2.

The unstable region appears to be similar in both heating temperature cases, i.e., increasing and decreasing, and is near the critical point of CO_2. In this study, this region is defined as an unstable region. Among the regions shown in Figure 7, flow instability was not observed in the topside and injection wellbore when the pressure and temperature are above those at the boundary of the regions.

Such an unstable region exhibits several characteristics. For example, the corresponding pseudocritical pressure is approximately 79.8 bar at a pseudocritical temperature of approximately 34.5 °C. The unstable regions can be distinguished using this value. In other words, the pressure should be higher than 79.8 bar ($P > Ppc$ = 79.8 bar) to prevent instability at a temperature lower than the pseudocritical temperature of approximately 34.5 °C ($T < Tpc$ = 34.5 °C). In addition, the pressure should be higher than 77 bar ($P > Ppc$ = 77 bar) to avoid instability above the pseudocritical temperature of approximately 34.5 °C ($T > Tpc$ = 34.5 °C).

Thus, the existence of an unstable CO_2 flow region in the pipeline suggests that the unstable flow must be considered in the design and operation of the entire CCS value chain in which CO_2 flows in the supercritical state. Considering the unstable flow, a specific range of operating conditions must be defined for system design and operation. Moreover, analytical results for critical and supercritical CO_2 that correspond to the unstable flow are required. The results of this study identify the specific region near the critical point where the CO_2 flow is unstable. CO_2 near the critical point is known to exhibit sudden changes in its properties even on small pressure and temperature variations based on existing studies and experiments. However, if the CO_2 transportation and injection system is operated in an unstable region, the cause of flow instability should be analyzed in detail. Thus, the changes in the properties of CO_2 in the unstable region and near the pseudocritical line were analyzed, as explained in detail in the next section.

3.2. Effect of Property Changes Near the Pseudocritical Region

Figures 8 and 9 show the unstable regions in the temperature–density and the pressure–density diagrams of CO_2, respectively. The unstable region is highlighted as the colored region. Furthermore, the instability boundaries which were obtained through the numerical simulations are also specified. The density of CO_2 changes rapidly even with a slight temperature change at the critical point and in the near-critical region, as shown in Figure 8.

Similarly, as shown in Figure 9, a rapid density change was observed, even with a slight pressure change at the critical point and in the near-critical region. However, the density change behavior occurs not only at the critical point and in the near-critical region but also in the supercritical region. For example, as shown in Figure 8, the density of CO_2 changes rapidly if there is a slight change in the pressure or temperature at supercritical conditions, i.e., a pressure of 78 bar and a temperature of 33.5 °C. Assuming that the temperature changes from 33 to 34 °C at a constant pressure of 78 bar, the change in the density of CO_2 is more than 300 kg/m^3. The unstable region includes an area with significant density variations because of temperature or pressure changes. The sudden changes in the properties are evident along the pseudocritical line, as shown in Figure 7 and reported in previous studies. In particular, the properties change abruptly near the pseudocritical line in the unstable region. In other words, in the CO_2 transportation and injection system analyzed in this study, if the operating pressure of the topside is in the unstable region and the heater outlet temperature is set to a temperature within the unstable region, the pressure or temperature of the heated CO_2 may change slightly because of the pressure drop or heat transfer in the pipeline, resulting in a significant change in the density.

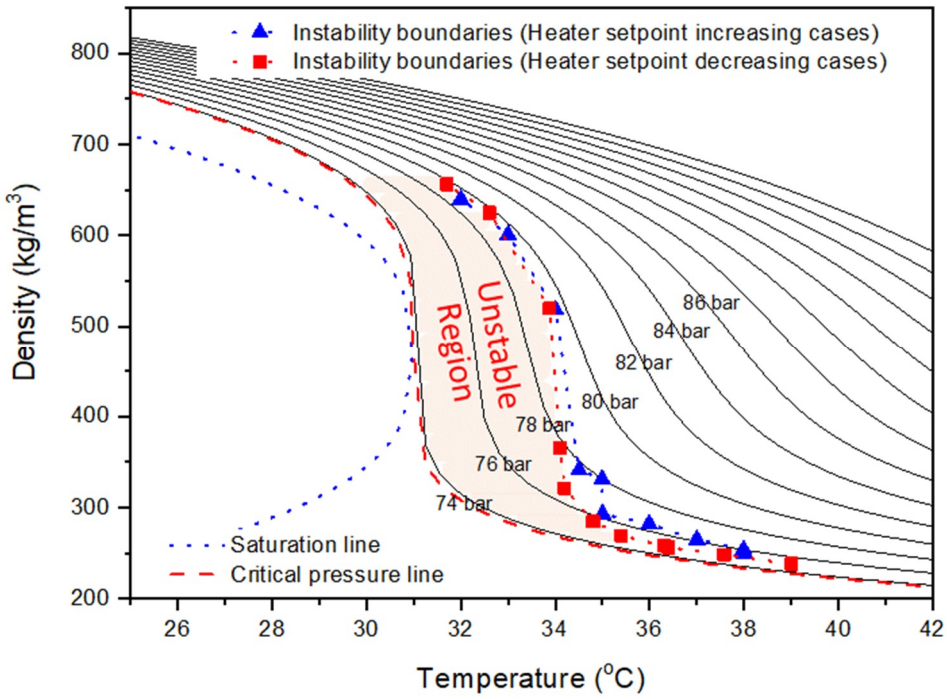

Figure 8. Temperature–density diagram of CO_2 with an unstable region.

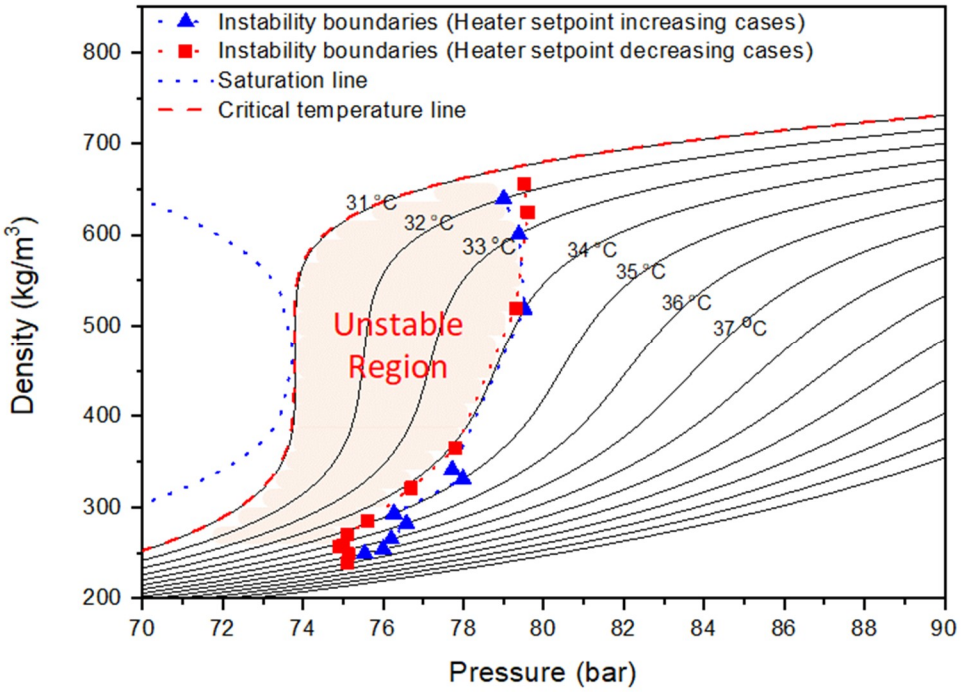

Figure 9. Pressure–density diagram of CO_2 with an unstable region.

To analyze the density behavior of CO_2 in the unstable region in more detail, the density gradient of CO_2 was plotted with respect to the pressure and temperature, as shown in Figures 10 and 11. The pressure and temperature ranges, shown in Figures 10 and 11, are within the previously obtained unstable region. Along the pseudocritical line in the unstable region, the density of CO_2 changes significantly depending on the pressure and temperature. The density gradient is considerable at the critical point, whereas it decreases as the temperature and pressure move away from the critical

point, i.e., outside the unstable region. In the aforementioned region, shown in Figure 7, the operating conditions, i.e., a pressure of 80.7 bar and a temperature of 35 °C, are located on the pseudocritical line; however, they are outside the unstable region. If the same logic is applied to the relationship shown in Figures 10 and 11, there is no notable density change in the pseudocritical line above 79.8 bar and 34.5 °C.

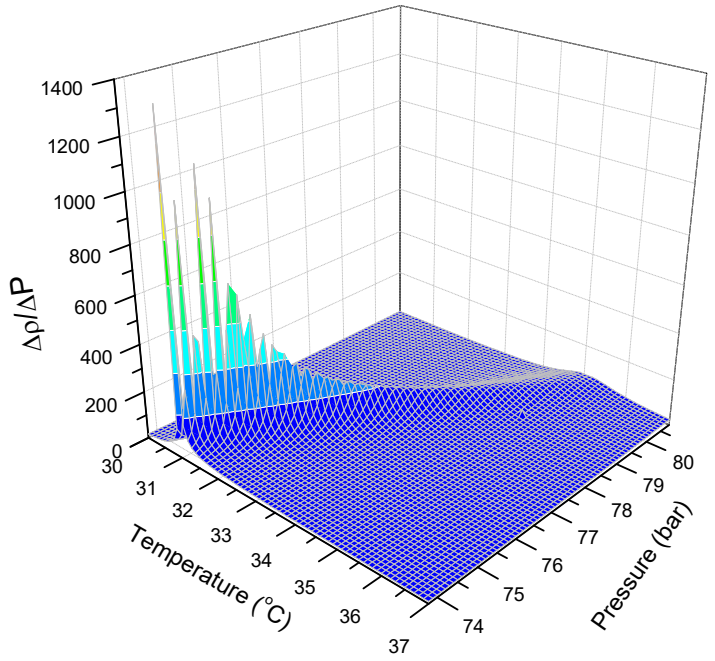

Figure 10. Density gradient of CO_2 with respect to pressure.

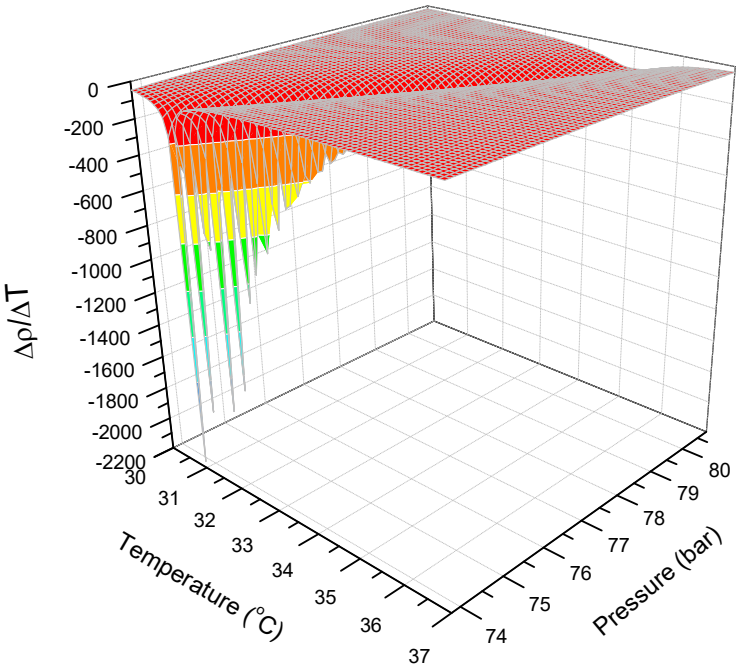

Figure 11. Density gradient of CO_2 with respect to temperature.

As shown in the CO_2 density gradient with respect to the pressure in Figure 10, the pressure and temperature at which the density gradient becomes a maximum lie on the pseudocritical line shown in Figure 7. At the critical point and in the near-critical region of CO_2, the density gradient

arising from the pressure increases sharply up to approximately 1000 kg/m^3·bar. On the other hand, the density gradient of CO_2 with respect to the temperature, as shown in Figure 11, decreases sharply to approximately 2100 kg/m^3·°C with increasing temperature. Figures 10 and 11 show that the density gradient of CO_2 on the pseudocritical line is more susceptible to temperature than to pressure.

The above results show that the density gradient of CO_2 with respect to the changes in the pressure and temperature changes rapidly in the unstable region. If this behavior occurs in the CO_2 transportation and injection system, a phenomenon similar to density wave oscillations arising from the difference in the densities of the liquid and vapor phases in two-phase flow may occur, even though CO_2 is in a single-phase supercritical state. This phenomenon is analyzed in Section 3.3.

3.3. Analysis of the Instability

Based on the results in the preceding section, CO_2 in the supercritical state near the critical point and in the unstable region shows an unstable state with rapid changes in its properties, even when the temperature and pressure change slightly. If these rapid changes in properties occur in the CO_2 transportation pipeline and injection wellbore, they can cause severe flow instability, possibly resulting in loss of flow control. In this section, the cause of the above-mentioned flow instability in the unstable region is analyzed.

Generally, in a two-phase flow system, density wave oscillations are due to the difference in the densities between the high-density liquid phase and the low-density vapor phase, and this can cause a sudden pressure drop or perturbation in the flow velocity, resulting in flow instability in the system [37]. However, the fluid density along the pseudocritical line can change rapidly even in a supercritical fluid, and this can also cause a phenomenon similar to density wave oscillation. Studies have shown that flow instability arising from the density difference occurs even in a supercritical single-phase water flow, which is similar to density wave oscillations in the two-phase flow of subcritical water [31]. The CO_2 flow instability in the supercritical state and in the near-critical region occurs in the single-phase supercritical region and is, thus, different from the density wave oscillation of the existing two-phase system. However, based on the results reported in the previous chapter, the density change of CO_2 occurring at the pseudocritical line in the unstable region appears to be similar to the density change behavior occurring at the saturation line. This resulted in a behavior similar to the flow instability arising from the phase change in a two-phase flow system.

In the supercritical CO_2 single-phase flow of this study, a phenomenon similar to the flow instability that occurs in two-phase flow because of the phase change of CO_2 was observed. Therefore, the calculation results of this study were applied to a stability map using two non-dimensional numbers: the sub-pseudo-critical number, N_{SUBPC}, and the trans-pseudo-critical number, N_{TPC}. The two dimensionless numbers have been used to describe the instability boundaries [38,39]. These two dimensionless numbers have been modified such that the phase change number, N_{PCH}, and the subcooling number, N_{SUB}, of the existing subcritical fluid stability map could be applied to a supercritical fluid [38]. A stability map that distinguishes between the stable and unstable flow regions can be obtained by calculating and plotting N_{SUBPC} (sub-pseudo-critical number) and N_{TPC} (trans-pseudo-critical number) of the supercritical fluid. The exact formulae are given in Equations (1) and (2), respectively.

$$N_{\mathrm{SUBPC}} = \frac{\beta_{pc}}{C_{p,pc}}\left(h_{pc} - h_{in}\right) \tag{1}$$

$$N_{TPC} = \frac{\dot{Q}}{\dot{m}}\frac{\beta_{pc}}{C_{p,pc}} \tag{2}$$

Here, β_{pc} is the coefficient of volume expansion at the pseudo-critical point, $C_{p,pc}$ is the specific heat at the pseudocritical point, h_{pc} is the enthalpy at the pseudocritical point, h_{in} is the enthalpy of CO_2 at the topside heater inlet, $\dot{Q}$ is the heat flow rate input from the topside heater, and $\dot{m}$ is the mass flow rate of CO_2 in the system.

In this study, the same temperature of the heater inlet condition, 5.7 °C, was applied, which is the topside arrival temperature, and h_{in} was calculated using the operating pressure and inlet temperature of every calculation case. The CO_2 properties were calculated using NIST's REFPROP [8]. For the flow rate of CO_2 used, a constant value of 31.5 kg/s was applied to the system. Furthermore, the amount of heat input to the heater was calculated for each simulation case.

The two non-dimensional numbers applied to this system were calculated separately and categorized into three groups: the operating conditions of the unstable region boundaries obtained above, operating conditions of the unstable region wherein the flow is unstable, and operating conditions outside the unstable region where the flow is stable.

The N_{SUBPC} value increases with increasing difference between the temperature corresponding to the pseudocritical enthalpy of the heater operating pressure and the temperature at the heater inlet. The N_{TPC} value tends to increase as the heater increasingly heats the CO_2. Figure 12 shows that the trend in the flow instability of supercritical CO_2 is clearly different at the boundary of the previously obtained unstable region.

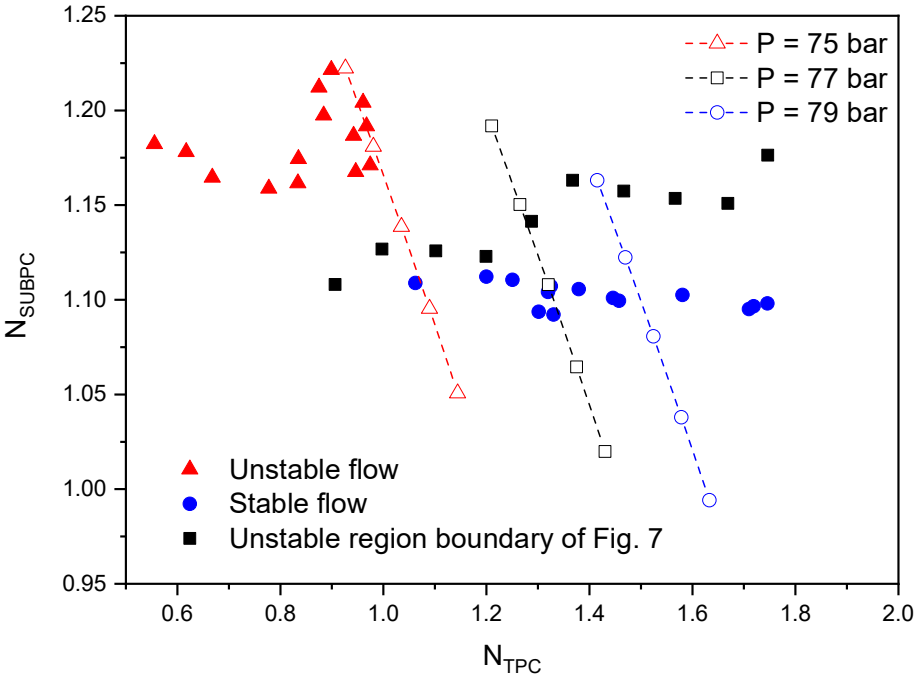

Figure 12. Stability map of supercritical CO_2.

As shown in Figure 12, the stability map obtained using the two dimensionless numbers indicates that the flow in the system becomes more unstable with increasing subcooling at the heater inlet, and the flow in the system becomes more stable as more heat is input to the heater. The effect of the inlet subcooling and the supplied heat at constant pressure is investigated. Table 3 shows the calculation conditions. As the subcooling increases (N_{SUBPC} increase), the flow becomes unstable. Furthermore, as more heat is supplied (N_{TPC} increase), the flow becomes more stable.

When the results, shown in Figure 12, are compared to the stability map of supercritical water obtained by Ambrosini and Sharabi [39], differences in the ranges of N_{SUBPC} and N_{TPC} values are observed; however, the flow instability trend was similar. The difference between the ranges of the two dimensionless numbers was caused by the significant differences in the properties of the supercritical water and supercritical CO_2 depending on the pressure and temperature.

Table 3. Simulation conditions for constant pressure case.

Inlet Pressure (bar)	Inlet Temperature (°C)	Mass Flowrate (kg/s)	Supplied Heat (kW)
75	5	31.5	3400
	7		3600
	9		3800
	11		4000
	13		4200
77	5	31.5	4400
	7		4600
	9		4800
	11		5000
	13		5200
77	5	31.5	5200
	7		5400
	9		5600
	11		5800
	13		6000

3.4. Case Study on CO_2 Pipeline Transport

A case study was conducted on a standard CO_2 pipeline to determine whether the results of this study were specific to a system that is heated by a topside heater, as in this study. To this end, a numerical analysis was carried out by modeling a 10 km-long horizontally installed pipeline used to transport CO_2. Table 4 outlines the calculation conditions for the numerical analysis of the CO_2 pipeline in each case. The same values for the pipeline diameter and flow rate as those of the existing system were used. The initial pressure and temperature in the pipeline were all outside the unstable region of the pipeline. As the simulation time passed from 10 h to 40 h, the outlet pressure of the pipeline decreased, and the operating conditions were within the unstable region. Through this process, we analyzed whether the flow instability occurs in the pipeline when the pipeline inlet with a high pressure operating condition is located outside the unstable region and when the pipeline outlet with a low pressure operating condition is located inside the unstable region.

Table 4. Simulation conditions for each horizontal pipeline case.

Case	Time (h)	Pipeline Length (km)	Temperature (Inlet–Outlet) (°C)	Pressure (Inlet–Outlet) (bar)
1	10	10	34.0–32.6	88.5–83.0
	20			86.7–81.0
	30			85.0–79.0
	40			81.0–77.1
2	10	10	36.0–34.0	88.2–82.0
	20			86.6–80.0
	30			85.0–78.0
	40			81.3–76.0
3	10	10	39.0–35.9	89.2–82.0
	20			87.8–80.0
	30			85.3–77.0
	40			84.9–75.0

Figure 13 shows the pressure–temperature diagram of CO_2, showing the pressure and temperature calculated at intervals of 10 h in the pipeline for each case study. In all three cases, the temperature and pressure fluctuated because the operating conditions near the pipeline outlet are located in the unstable region. This fluctuation shows that the flow instability spreads to all pipeline sections. Consequently,

the abnormal pressure and temperature profiles were shown in 40 h, see Figure 13. Concerning the cause of the flow instability mentioned above, the rapid changes in the CO_2 properties at the pipeline outlet affected the entire pipeline. This result suggests that the unstable CO_2 region at the critical point and in the near-critical region obtained from this study affects the flow instability of general pipelines. In other words, the unstable behavior of CO_2 in the unstable region not only occurs when it is heated by a heat exchanger, such as the heater used in this study, but also in more general cases.

If the temperature and pressure of the fluid are within the unstable region in a specific section of the CO_2 transportation and injection system, the conditions are sufficient to cause flow instability in the entire system. Therefore, the operating conditions of the CO_2 transportation and injection system should be designed in such a manner to avoid the unstable region, as shown in the results of this study.

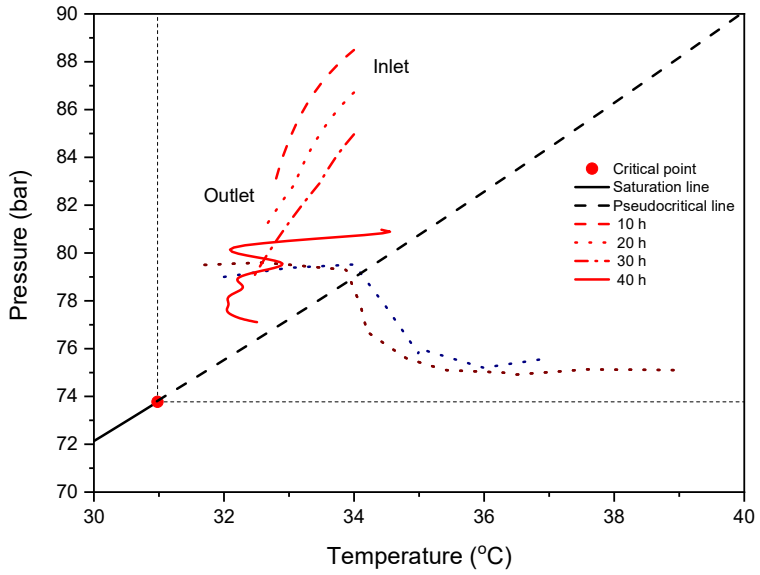

(**a**) Case 1

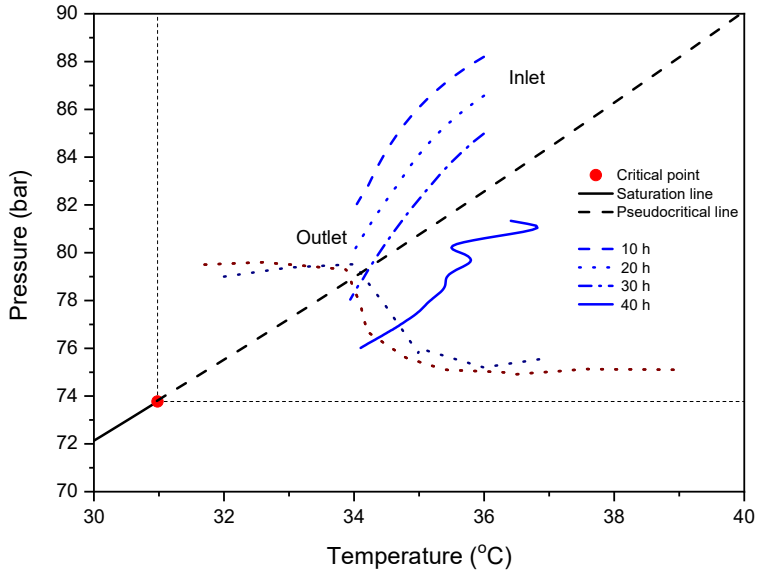

(**b**) Case 2

Figure 13. *Cont.*

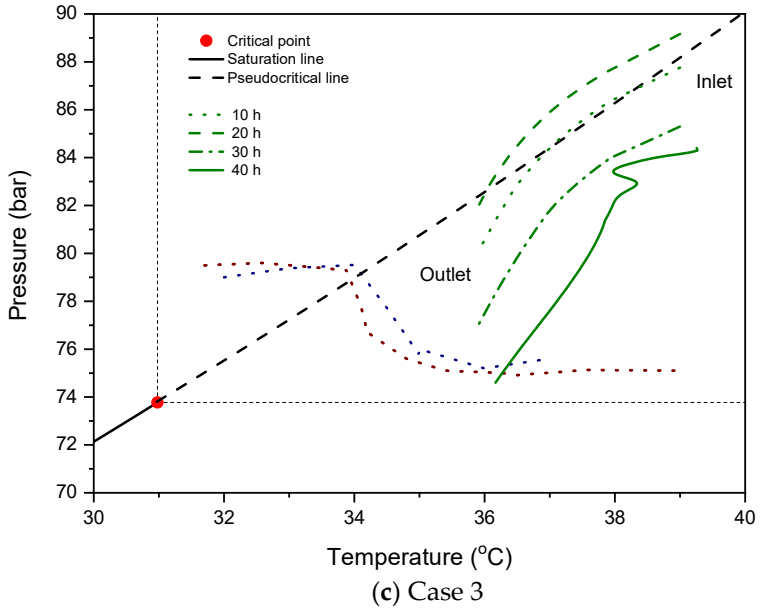

(**c**) Case 3

Figure 13. Pressure–temperature profile of the horizontal pipeline.

4. Conclusions

The CO_2 captured in CCS systems is in a subcritical state at room temperature and atmospheric pressure and is stored in a supercritical state in the subsurface reservoir because of the geothermal heat and hydrostatic pressure. In other words, there is a phase difference between the captured and stored CO_2, suggesting that a phase transition between the gas and liquid phases and the transition from subcritical to supercritical can occur in a CO_2 transportation and injection system. In transportation and injection systems operating under these conditions, even slight changes in the operating conditions and the external environmental conditions can lead to significant changes in the temperature and pressure of the CO_2. The changes in the temperature and pressure at the supercritical point and in a region near the pseudocritical line can lead to rapid changes in the properties, thus causing flow instability in the entire transportation and injection system. Therefore, in this study, the CO_2 flow instability was identified at the critical point and in the near-critical region during the CO_2 transportation and injection process, and its causes and effects were analyzed. It should be noted that this study has primarily concentrated on a numerical analysis of the CO_2 flow instability associated with the critical point and near-critical region. Nevertheless, experimental verification of the aforementioned unstable behavior would be helpful, and this will be considered in future research. The main conclusions from the results of this study are as follows.

(1) The regions corresponding to the operating conditions causing flow instability were categorized into four areas; at the critical point, in the near-critical region, in a region near the pseudocritical line, and in the supercritical region. The pressure must be higher than 80 bar ($P > Ppc = 80$ bar) to prevent instability at temperatures lower than the pseudocritical temperature of ca. 34.5 °C ($T < Tpc = 34.5$ °C). Furthermore, the pressure must be at least 77 bar ($P > Ppc = 77$ bar) to avoid instability at temperatures higher than the pseudocritical temperature of ca. 34.5 °C ($T > Tpc = 34.5$ °C).

(2) The density of CO_2 in the unstable region varies rapidly depending on the temperature and pressure. The rapid change in the density of CO_2 caused by the operating conditions in the unstable region caused an unstable flow with a trend similar to that of density wave oscillations resulting from the phase change in subcritical two-phase flow, even though the studied condition is a supercritical single-phase fluid.

(3) To describe the instability boundaries, the stability map was developed using the two dimensionless numbers which are the sub-pseudocritical number (N_{SUBPC}) and the trans-pseudo-critical number (N_{TPC}). The stability map revealed that the trends of the flow instability in CCS were similar with supercritical water.

(4) To verify whether the unstable region obtained in this study is specific only to the case of heating with the heater, additional numerical analysis was conducted on three horizontal pipelines. In all three cases, the flow instability of CO_2 was observed when the operating conditions entered the unstable region. Therefore, the unstable region of this study can be applied to the design of standard CO_2 pipelines. In other words, the results of this study can be used for safe and economic CO_2 transportation and the design of CO_2 pipelines.

Author Contributions: Conceptualization, C.H.; Simulation and Analysis, I.H.M. and C.H.; Funding Acquisition, S.-G.K.; Writing—Original Draft Preparation, I.H.M. and C.H.; Writing—Review & Editing, C.H.

Funding: This research was supported by a grant [KCG-01-2017-05] through the Disaster and Safety Management Institute funded by Korea Coast Guard of the Korean government and by the National Research Foundation of Korea (NRF) grant funded by the Korea government (Ministry of Science and ICT) (2017R1E1A1A03070672).

Acknowledgments: The authors would like to thank Schlumberger for their donation of OLGA.

Conflicts of Interest: The authors declare no conflict of interest.

References

1. Metz, B.; Davidson, O.; de Coninck, H.; Loos, M.; Meyer, L. *IPCC Carbon Dioxide Capture and Storage*; Cambridge University Press: Cambridge, UK, 2005.
2. Huh, C.; Kang, S.-G.; Park, M.-H.; Lee, K.-S.; Park, Y.-G.; Min, D.-J.; Lee, J.-S. Latest CO_2 transport, storage and monitoring R&D progress in Republic of Korea: Offshore geologic storage. *Energy Procedia* **2013**, *37*, 6520–6526.
3. Min, I.H.; Huh, C. Development of new CO_2 heating process for offshore geological storage. *Int. J. Greenh. Gas Control* **2017**, *64*, 1–10. [CrossRef]
4. Kang, K.; Seo, Y.; Chang, D.; Kang, S.-G.; Huh, C. Estimation of CO_2 transport costs in South Korea using a techno-economic model. *Energies* **2015**, *8*, 2176–2196. [CrossRef]
5. Min, I.H.; Huh, C.; Choe, Y.S.; Kim, H.U.; Cho, M.I.; Kang, S.G. Numerical analysis of CO_2 behavior in the subsea pipeline, topside and wellbore with reservoir pressure increase over the injection period. *J. Korean Soc. Mar. Environ. Energy* **2016**, *19*, 286–296. [CrossRef]
6. Pioro, I.; Mokry, S. Thermophysical properties at critical and supercritical conditions. In *Heat Trasnfer: Theoretical Analysis, Experimental Investigations and Industrial Systems*; Belmiloudi, A., Ed.; IntechOpen: Vienna, Austria, 2007; pp. 573–592.
7. Lamorgese, A.; Ambrosini, W.; Mauri, R. Widom line prediction by the Soave–Redlich–Kwong and Peng–Robinson equations of state. *J. Supercrit. Fluids* **2018**, *133*, 367–371. [CrossRef]
8. Lemmon, E.W.; Huber, M.L.; McLinden, M.O. *NIST Standard Reference Database 23: Reference Fluid Thermodynamic and Transport Properties-REFPROP*; version 9.1; NIST: Gaithersburg, MD, USA, 2013.
9. Tian, R.; An, Q.; Zhai, H.; Shi, L. Performance analyses of transcritical organic Rankine cycles with large variations of the thermophysical properties in the pseudocritical region. *Appl. Therm. Eng.* **2016**, *101*, 183–190.
10. Cabeza, L.F.; de Gracia, A.; Fernández, A.I.; Farid, M.M. Supercritical CO_2 as heat transfer fluid: A review. *Appl. Therm. Eng.* **2017**, *125*, 799–810. [CrossRef]
11. Shoaib, A.M.; Bhran, A.A.; Awad, M.E.; El-Sayed, N.A.; Fathy, T. Optimum operating conditions for improving natural gas dew point and condensate throughput. *J. Nat. Gas Sci. Eng.* **2018**, *49*, 324–330. [CrossRef]
12. Guerrero-Zárate, D.; Estrada-Baltazar, A.; Iglesias-Silva, G.A. Calculation of critical points for natural gas mixtures with the GERG-2008 equation of state. *Fluid Phase Equilib.* **2017**, *437*, 69–82. [CrossRef]

13. Wang, T.; Ding, C.; Ding, G.; Zhao, D.; Ren, T. A fast calculation method of thermodynamic properties of variable-composition natural gas mixtures in the supercritical pressure region based on implicit curve-fitting. *J. Nat. Gas Sci. Eng.* **2017**, *43*, 96–109. [CrossRef]
14. Chaczykowski, M.; Zarodkiewicz, P. Simulation of natural gas quality distribution for pipeline systems. *Energy* **2017**, *134*, 681–698. [CrossRef]
15. Wang, P.; Yu, B.; Deng, Y.; Zhao, Y. Comparison study on the accuracy and efficiency of the four forms of hydraulic equation of a natural gas pipeline based on linearized solution. *J. Nat. Gas Sci. Eng.* **2015**, *22*, 235–244. [CrossRef]
16. Pambour, K.A.; Bolado-Lavin, R.; Dijkema, G.P.J. An integrated transient model for simulating the operation of natural gas transport systems. *J. Nat. Gas Sci. Eng.* **2016**, *28*, 672–690. [CrossRef]
17. Guandalini, G.; Colbertaldo, P.; Campanari, S. Dynamic modeling of natural gas quality within transport pipelines in presence of hydrogen injections. *Appl. Energy* **2017**, *185*, 1712–1723. [CrossRef]
18. Ma, Y.; Liu, M.; Yan, J.; Liu, J. Thermodynamic study of main compression intercooling effects on supercritical CO_2 recompression Brayton cycle. *Energy* **2017**, *140*, 746–756. [CrossRef]
19. Shao, L.L.; Zhang, C.L. Thermodynamic transition from subcritical to transcritical CO_2 cycle. *Int. J. Refrig.* **2016**, *64*, 123–129. [CrossRef]
20. Gupta, S.; Saltanov, E.; Mokry, S.J.; Pioro, I.; Trevani, L.; McGillivray, D. Developing empirical heat-transfer correlations for supercritical CO_2 flowing in vertical bare tubes. *Nucl. Eng. Des.* **2013**, *261*, 116–131. [CrossRef]
21. Han, S.H.; Chang, D.; Huh, C. Efficiency analysis of radiative slab heating in a walking-beam-type reheating furnace. *Energy* **2011**, *36*, 1265–1272. [CrossRef]
22. Chen, Q.; Zhao, S.Y.; Chen, X.; Li, X. The power flow topology of heat transfer systems at supercritical conditions for performance analysis and optimization. *Int. J. Heat Mass Transf.* **2018**, *118*, 316–326. [CrossRef]
23. Ma, T.; Chu, W.X.; Xu, X.Y.; Chen, Y.T.; Wang, Q.W. An experimental study on heat transfer between supercritical carbon dioxide and water near the pseudo-critical temperature in a double pipe heat exchanger. *Int. J. Heat Mass Transf.* **2016**, *93*, 379–387. [CrossRef]
24. Rao, N.T.; Oumer, A.N.; Jamaludin, U.K. State-of-the-art on flow and heat transfer characteristics of supercritical CO_2 in various channels. *J. Supercrit. Fluids* **2016**, *116*, 132–147. [CrossRef]
25. Archana, V.; Vaidya, A.M.; Vijayan, P.K. Flow transients in supercritical CO_2 natural circulation loop. *Procedia Eng.* **2015**, *127*, 1189–1196. [CrossRef]
26. Chen, L.; Zhang, X.R.; Yamaguchi, H.; Liu, Z.S. Effect of heat transfer on the instabilities and transitions of supercritical CO_2 flow in a natural circulation loop. *Int. J. Heat Mass Transf.* **2010**, *53*, 4101–4111. [CrossRef]
27. Swapnalee, B.T.; Vijayan, P.K.; Sharma, M.; Pilkhwal, D.S. Steady state flow and static instability of supercritical natural circulation loops. *Nucl. Eng. Des.* **2012**, *245*, 99–112. [CrossRef]
28. Liu, G.; Huang, Y.; Wang, J.; Lv, F.; Liu, S. Experimental research and theoretical analysis of flow instability in supercritical carbon dioxide natural circulation loop. *Appl. Energy* **2017**, *205*, 813–821. [CrossRef]
29. Chen, L.; Zhang, X.R.; Deng, B.L.; Jiang, B. Effects of inclination angle and operation parameters on supercritical CO_2 natural circulation loop. *Nucl. Eng. Des.* **2013**, *265*, 895–908. [CrossRef]
30. Zuber, N. *An Analysis of Thermally Induced Flow Oscillations in the Near-Critical and Supercritical Thermodynamic Region*; NASA: Huntsville, AL, USA, 1966.
31. Ambrosini, W. On the analogies in the dynamic behaviour of heated channels with boiling and supercritical fluids. *Nucl. Eng. Des.* **2007**, *237*, 1164–1174. [CrossRef]
32. Xiong, T.; Yan, X.; Xiao, Z.; Li, Y.; Huang, Y.; Yu, J. Experimental study on flow instability in parallel channels with supercritical water. *Ann. Nucl. Energy* **2012**, *48*, 60–67. [CrossRef]
33. KRISO. *Whole CCS System Operation Philosophy, Korea Clean Carbon Storage Project 2025 Pre-FEED Report*; KRISO: Dae-jeon, Korea, 2016.
34. Schlumberger OLGA Dynamic Multiphase Flow Simulator. Available online: http://www.software.slb.com/products/foundation/Pages/olga.aspx (accessed on 3 September 2014).
35. Huh, C.; Cho, M.I.; Kang, S.G. Numerical analysis on depressurization of high pressure carbon dioxide pipeline. *J. Korean Soc. Mar. Environ. Energy* **2016**, *19*, 52–61. [CrossRef]
36. KNOC. *Carbon Storage Potential in the Ulleung Basin, South Korea: Prospect Modelling and Ranking*; KNOC: Ulsan, Korea, 2015.

37. Dorao, C.A. Effect of inlet pressure and temperature on density wave oscillations in a horizontal channel. *Chem. Eng. Sci.* **2015**, *134*, 767–773. [CrossRef]
38. Su, Y.; Feng, J.; Zhao, H.; Tian, W.; Su, G.; Qiu, S. Theoretical study on the flow instability of supercritical water in the parallel channels. *Prog. Nucl. Energy* **2013**, *68*, 169–176. [CrossRef]
39. Ambrosini, W.; Sharabi, M. Dimensionless parameters in stability analysis of heated channels with fluids at supercritical pressures. *Nucl. Eng. Des.* **2008**, *238*, 1917–1929. [CrossRef]